Overview of Bering and Chukchi Sea Wave States for Four Severe Storms following Common Synoptic Tracks

KATHERINE A. PINGREE-SHIPPEE

International Arctic Research Center, and Arctic Region Supercomputing Center, University of Alaska Fairbanks, Fairbanks, Alaska, and Department of Geography, and Pacific Climate Impacts Consortium, University of Victoria, Victoria, British Columbia, Canada

NORMAN J. SHIPPEE AND DAVID E. ATKINSON

Department of Geography, University of Victoria, Victoria, British Columbia, Canada, and International Arctic Research Center, University of Alaska Fairbanks, Fairbanks, Alaska

(Manuscript received 28 July 2015, in final form 24 October 2015)

ABSTRACT

Strong storms occur regularly over the ocean west of Alaska. These systems often loiter, generating persistent winds that can result in fully developed marine states that can maximize damage and hazard potential. Detailed analyses of storm events in terms of the resultant wave states are uncommon. This analysis examines the wave states associated with four particular storm events over the Bering and Chukchi Seas: October 2004, September 2005, and November 2009, and a September 2011 event that exhibited north winds. For each event a brief synoptic overview is presented followed by consideration of the resultant wave state, including parameters such as wave steepness. Wave data come from NOAA's WAVEWATCH III (WW3) operational global ocean wave model, implemented for scenario use at the Arctic Region Supercomputing Center at the University of Alaska Fairbanks. In situ data are available from several National Data Buoy Center buoys and a wave buoy located in the Bering Strait, funded by the U.S. Environmental Protection Agency and NOAA and deployed for a few months in 2011. WW3 accurately captures the timing and evolution of the observed wave action (onset, growth, peak, and decline of large, steep wind waves) for each of the storm events. As per previous climatologically oriented studies, WW3 is found to underestimate significant wave heights on the order of 0.5 m or less. Also larger discrepancies, on the order of 1–2 m, are observed during periods of peak significant wave heights (Hs). In some cases WW3 overestimated Hs, especially during periods of rapid Hs decline.

1. Introduction

Strong storms over the Bering and Chukchi Seas (Fig. 1a) are common occurrences, and they often result in adverse impacts and damage along the Alaskan coastal region. Over the eastern Bering Sea, storms often stall, creating severe, persistent wave states and possible storm surge conditions, bringing hazards to shipping and hunting activities, coastal flooding, erosion, and structural damage amounting to millions of dollars. These storms often produce winds up to 35 m s^{-1} with gusts up to 45 m s^{-1}, wind waves exceeding 10 m, storm surges approaching 4 m, and resultant local surge plus wave water levels elevated upward of 7 m (Sallenger 1983; Kowalik 1984; Johnson and Kowalik 1986; Blier et al. 1996; Mason et al. 1996). In winter, these storms bring blizzard conditions, break up landfast ice, and push sea ice into harbors and onto the shore. For example, back-to-back severe storms moved through the Bering Sea between 9 and 12 November 1974, resulting in the worst coastal flooding of the southern Seward Peninsula observed in 60 years, with notable flooding reported in the major coastal Alaskan hub communities of Nome, Unalakleet, and Kotzebue (Fathauer 1975). The first storm, which moved along a northeastward track through the Bering Sea on 10 November 1974, had

Corresponding author address: Katherine Pingree-Shippee, Pacific Climate Impacts Consortium, University of Victoria, University House 1, P.O. Box 1700 Stn CSC, Victoria BC V8W 3R4, Canada.
E-mail: kpingree@uvic.ca

DOI: 10.1175/JTECH-D-15-0153.1

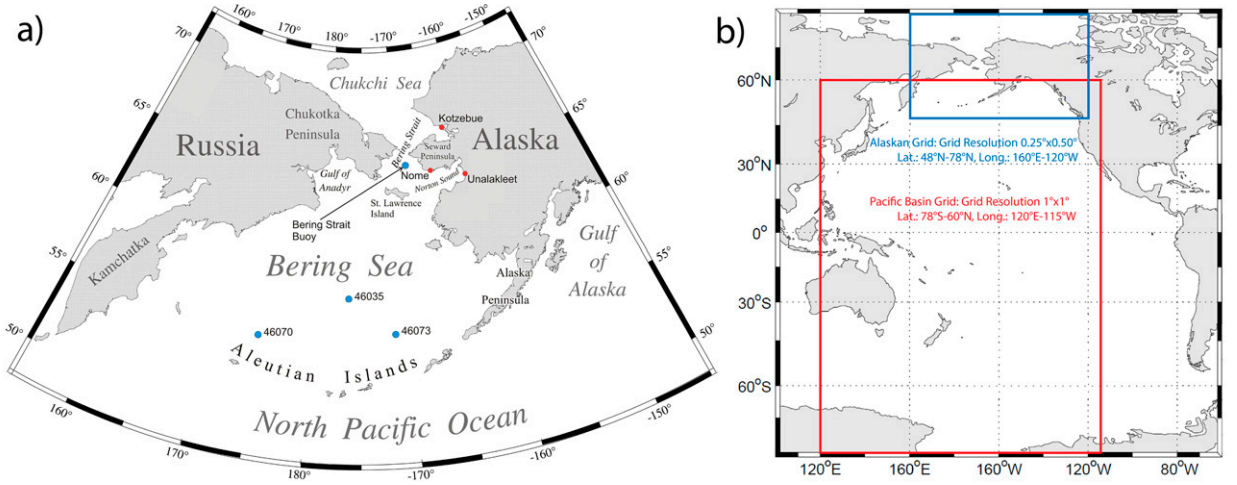

FIG. 1. (a) Study domain and locations of permanent Bering Sea buoys and temporary "Bering Strait buoy": buoy 46070—55.083°N, 175.270°E; buoy 46035—57.067°N, 177.750°W; buoy 46073—55.011°N, 171.981°W; Bering Strait Buoy—65.000°N, 168.750°W. (b) WW3 nested Pacific and Alaskan grids.

a minimum central pressure of 984 hPa and produced heavy snow and high winds up to 27 m s^{-1}. The second storm was much more powerful. It moved along a northerly track through the Bering Sea on 11 November 1974, dropped to a central pressure of 949 hPa at peak strength, and produced winds approaching 40 m s^{-1} (Fathauer 1975). Combined, these storms generated a local sea level rise of approximately 1.8–3.7 m, causing flooding along northwestern Alaska, which resulted in an estimated $12–$15 million in damages to Nome alone (Fathauer 1975). Such events are not uncommon. During 8–10 November 2011, a comparable storm moved through the Bering and Chukchi Seas. It exhibited a central pressure minima of 944 hPa and brought hurricane-strength winds, blizzard conditions, and coastal flooding, causing widespread damage exceeding $24 million, and affecting approximately 1500 km of coastline and more than 35 communities (NCDC 1999). Such an event is a heavy blow for a region with a population of less than 50 000, no roads connecting to the interior or major cities, and limited economic resiliency.

Previous research on storm activity in the Bering and Chukchi Seas region has primarily focused on the long-term climatology, characteristics (e.g., frequency and intensity), dynamics, and impacts of synoptic-scale storm activity (Overland and Pease 1982; Serreze et al. 1993; Hufford and Partain 2005; Rodionov et al. 2007; Simmonds et al. 2008; Mesquita et al. 2010; Simmonds and Rudeva 2014). For example, Mesquita et al. (2010) investigated extratropical cyclones traversing the North Pacific and Bering Sea regions over 1948–2008, focusing on the climatological properties of storm genesis, lysis, intensity, track density, and interseasonal variability trends. As a result of this work and other studies, the typical tracks of cyclones impacting the Bering and Chukchi Seas and western Alaska are generally well known and typically follow three tracks: 1) north/north-northeastward following the coast of Siberia; 2) northeastward, across the Aleutian Islands, into the Bering Sea and continuing northward through the central Bering Sea; and 3) eastward, into the very southern Bering Sea, paralleling the Aleutian Island chain.

Climatological descriptions of storm parameters, however, are unable to provide information about individual storm events, which is of importance and interest to marine activities and coastal regions. Some previous studies have focused on individual synoptic events but the resulting sea state is generally not the primary objective. For example, Mesquita et al. (2009) focused on the severe October 1992 storm that strongly impacted the coastal community of Nome. That study, however, sought to contrast two cyclone tracking algorithms and to provide a detailed synoptic description of the event, and, thus, information about the resultant sea states was not included. The few studies that do focus on the sea state associated with storm events (Francis and Atkinson 2012a,b) and the resulting storm surges impacting the Alaskan coastline (Blier et al. 1997; Hufford and Partain 2005; Lynch et al. 2008) are limited in the extent of their coverage and representation of the resulting sea states. For instance, Francis and Atkinson (2012a,b) focus only on the southeast Chukchi Sea region for the 2007 and 2009–10 time periods, respectively.

A major reason why examinations of sea-state responses to synoptic events are not more common for the Bering/Chukchi Sea region is a lack of observational data.

NOAA operates three permanent buoys in the southern Bering Sea (Fig. 1a). These buoys possess relatively long records—station 46070, from 2006 onward; station 46035, from 1985 onward; and station 46073, from 2005 onward. While other organizations, such as Shell Arctic and the University of Alaska Fairbanks, have deployed buoys seasonally at higher latitudes in the ocean west of Alaska, annual sea ice prevents the use of permanent buoys in much of the region. Individual short-term (e.g., one season or year) datasets for surface waves have also been obtained from temporarily deployed equipment, such as the recording Doppler current profilers (RDCPs) utilized by Francis and Atkinson (2012a,b).

Wave data obtained from models can also be used to analyze wave-state response to storms. NOAA's WAVEWATCH III (WW3) global ocean wave model is useful in this regard because the source code is available and it has a well-established validation track record. Previous validation efforts that have included the Alaska region (in particular, the Bering Sea and the Gulf of Alaska) indicate that modeled significant wave heights are generally underestimated (Chawla et al. 2009, 2011; Spindler and Tolman 2010; Stopa and Cheung 2014). These studies consist of climatological evaluations of the wave states, they do not perform analyses on a storm-by-storm basis, and they primarily use altimeter data for validation. Chawla et al. (2009) conducted a global assessment that included a focus on the Gulf of Alaska and Bering Sea areas, with validation efforts in the Bering Sea limited to altimeter data; the only buoys utilized to represent the Alaska region were located in the Gulf of Alaska. The Chawla et al. (2011) validation also primarily utilized altimeter data (select buoys were included for validation outside the Alaska region), and it included the Bering and Chukchi Seas (when data were available). The Spindler and Tolman (2010) evaluation for the Alaska region did utilize buoy station 46035 (in the central Bering Sea), but their focus was on the near-coastal regions and the shallow-water buoys in the Gulf of Alaska. Similar to the Chawla et al. (2009) study, Stopa and Cheung (2014) also conducted a global assessment with validation efforts in the Alaska region utilizing buoys in the Gulf of Alaska and altimeter data in the Bering Sea. While Stopa and Cheung do provide model bias as a function of wave height, these results are limited for several reasons: it is an aggregate validation, the "Alaska region" only represents the Gulf of Alaska when using buoy data, and yearly aggregates are provided using altimeter data.

Thus, two gaps are evident in existing WW3 validation efforts in the context of the Alaska region. First, validation work has not considered individual storm events. Aggregate validation efforts provide climatological results that obscure the effects of individual events. As well, previous work has considered only significant wave heights (Hs) and not peak waves. Second, focus on the Bering and Chukchi Seas has been limited. Most studies that have included a region termed "Alaska" are confined to the Gulf of Alaska. This is a problem because the Bering and Chukchi Seas represent a unique region with regard to vulnerable end users—subsistence hunting, commercial fishing, industrial shipping and exploration, emergency response, tourism—who operate small craft and are strongly impacted by individual storm events, and who are reliant on products such as WW3 for decision-making. These seas are also somewhat enclosed and so less affected by swell conditions than areas south of the Aleutians, making locally generated wind waves the primary marine hazard.

Given the sensitivity of marine operators on the Bering and Chukchi Seas and the frequency and severity of storms, and the changes to storm activity in recent decades (Simmonds et al. 2008; Simmonds 2015), it is important to understand the evolution of wave states driven by particular storm events. The spatial patchiness of observational data means that modeled wave data must be used to fill in the gaps; WW3 is the best system for this. However, given that existing WW3 verification efforts have only been conducted at the climatological level, event-level verification should be performed for those parameters of most relevance to end users. To this end, this research effort has two objectives. First, perform a targeted analysis of the sea states and their synoptic drivers in the Bering and Chukchi Seas for four major storms. The analysis focuses on three sea-state variables of importance to end users—significant wave height, peak wave height, and wave steepness (ratio of wave height to wavelength, providing an indication of wave stability with steeper waves representing greater marine hazard). The analysis is performed using NOAA's WW3 model, implemented for scenario use at the Arctic Region Supercomputing Center at the University of Alaska Fairbanks. Second, conduct a limited validation of WW3 significant wave height output via comparisons to observational data from buoys located in the Bering Sea and a seasonally deployed buoy in the northern shelf area of the Bering Sea. This validation effort differs from those of Chawla et al. (2009, 2011) and Spindler and Tolman (2010), who examined the general (aggregate) response of WW3 using validation data, primarily altimeter, and were confined to the southern Bering Sea. WW3 has also been previously analyzed from the modeling perspective (e.g., output accuracy using different wind resolution data to drive the model) and sources of bias (Spindler and Tolman 2010; Durrant et al. 2013; Stopa and Cheung 2014) and

TABLE 1. Percentile ranking of peak reanalysis wind speed at 0.995σ during the storm events for each buoy location. Climatology wind distributions for 1979–2010 were developed using the NCEP Climate Forecast System Reanalysis (CFSR), and peak winds used to calculate percentile rankings are from CFSR (2004, 2005, and 2009 events) and NCEP Climate Forecast System, version 2 (CFSv2; 2011 event). CFSv2 was used for 2011 because CFSR data are not available for September 2011.

		Storm event			
		Oct 2004	Sep 2005	Nov 2009	Sep 2011
Buoy	46070	—	—	—	85.07
	46035	99.14	93.55	99.96	90.56
	46073	—	99.45	99.97	—
	Bering Strait	—	—	—	99.75

has been tuned for the overall Alaskan region (Tolman 2008; Spindler and Tolman 2010). As such, the intent of the present study is not to perform a comprehensive evaluation of the model in order to identify sources of bias (e.g., wind forcing vs model parameterizations), to determine the percentage of bias associated with input data (wind) resolution, or to further tune the model for the Bering/Chukchi Sea region. Instead, the intent is to determine, for particular storm events, whether WW3 wave heights exhibit the same biases as have been established from aggregate validation efforts, and to examine WW3 peak wave response.

The remainder of the paper is organized as follows: section 2 provides brief descriptions of the selected storms; sections 3 and 4 describe the WW3 global ocean wave model and the Bering Sea buoys used for validation, respectively. In section 5, descriptions of the storm events and associated wave states are presented. Finally, discussion and conclusions are provided in section 6.

2. Selected storms

Four recent major storms were selected for sea-state analysis: October 2004, September 2005, November 2009, and September 2011. Minimum central pressures were 941, 966, 960, and 955 hPa, respectively. These storms were selected for several reasons. First, and in particular, they resulted in notable physical and socioeconomic impacts for the Alaskan coastal region (e.g., coastal flooding and erosion, damage to residential and commercial structures), and while strong (see Table 1), they are not meant to represent the strongest storms ever recorded in the region. Rather, they constitute storms on the severe end of what might be expected in any given year. Second, they represent a cross section of common trajectories into this region. Third, they are meant to represent events exhibiting southerly flow (three events) and northerly flow (September 2011 event). As well, the 2011 event was selected to also take advantage of data from the Bering Strait buoy. The synoptic progression of these storms is described below. Socioeconomic impacts are also briefly discussed. Storm dates and peak strengths as used in this paper were classified using a combination of sea level pressure and significant wave heights.

a. October 2004 storm

A low pressure system (S04) moved north over the central Aleutian Islands into the Bering Sea on the evening of 17 October 2004 (Fig. 2a; note Alaska daylight time is −0800 UTC). Twenty-four hours later, the system had "bombed" and the central pressure had dropped by 37 to 941 hPa, its lowest reported value, centered over the Gulf of Anadyr. The storm then began to slowly weaken on 19 October, with the central pressure increasing to 980 hPa by 20 October. At this point, the system continued to loiter over the Gulf of Anadyr–Chukotka Peninsula region for the next ~24 hours before tracking over the Chukchi Sea. For this study, the storm dates considered cover 18–24 October 2004; this captures the time from peak strength through its period of impact in the Bering Sea. Although the storm reached peak strength based on sea level pressure on 18 October, maximum significant wave heights were observed on the following day; therefore, 19 October is considered the peak of the storm in this study. The storm produced winds of up to 36 m s^{-1} and storm surges up to 3.7 m. The resulting damage across coastal western Alaska was estimated at $20 million with the coastal community of Nome sustaining the majority of the damage. Regional damage included coastal flooding, structural damage to residential and commercial buildings, roadway damage, seawall and jetty damage in harbors, and minor damage to village water treatment systems (NCDC 1999).

b. September 2005 storm

A low pressure system (S05) moved north over the east-central Bering Sea on 22 September 2005 (Fig. 2b). By early on 23 September, the storm had strengthened to its minimum reported central pressure of 966 hPa and was located over the northern Bering Sea–Bering Strait. There the system stalled for approximately 3 days. In this study, storm dates are considered 21–26 September 2005, during which the storm reached peak strength on 23 September. The storm produced wind gusts of ~29 m s^{-1} in the coastal regions of Norton Sound (Fig. 1a) and the southern Chukchi Sea. Aided by the already elevated sea levels due to a weaker storm that had moved through one day earlier, 2.7-m storm surges and 3–4.6-m wind waves were reported in the northern Bering Sea, and 1.2-m storm surges and 1.5–3-m wind waves were reported in the southern Chukchi Sea. The

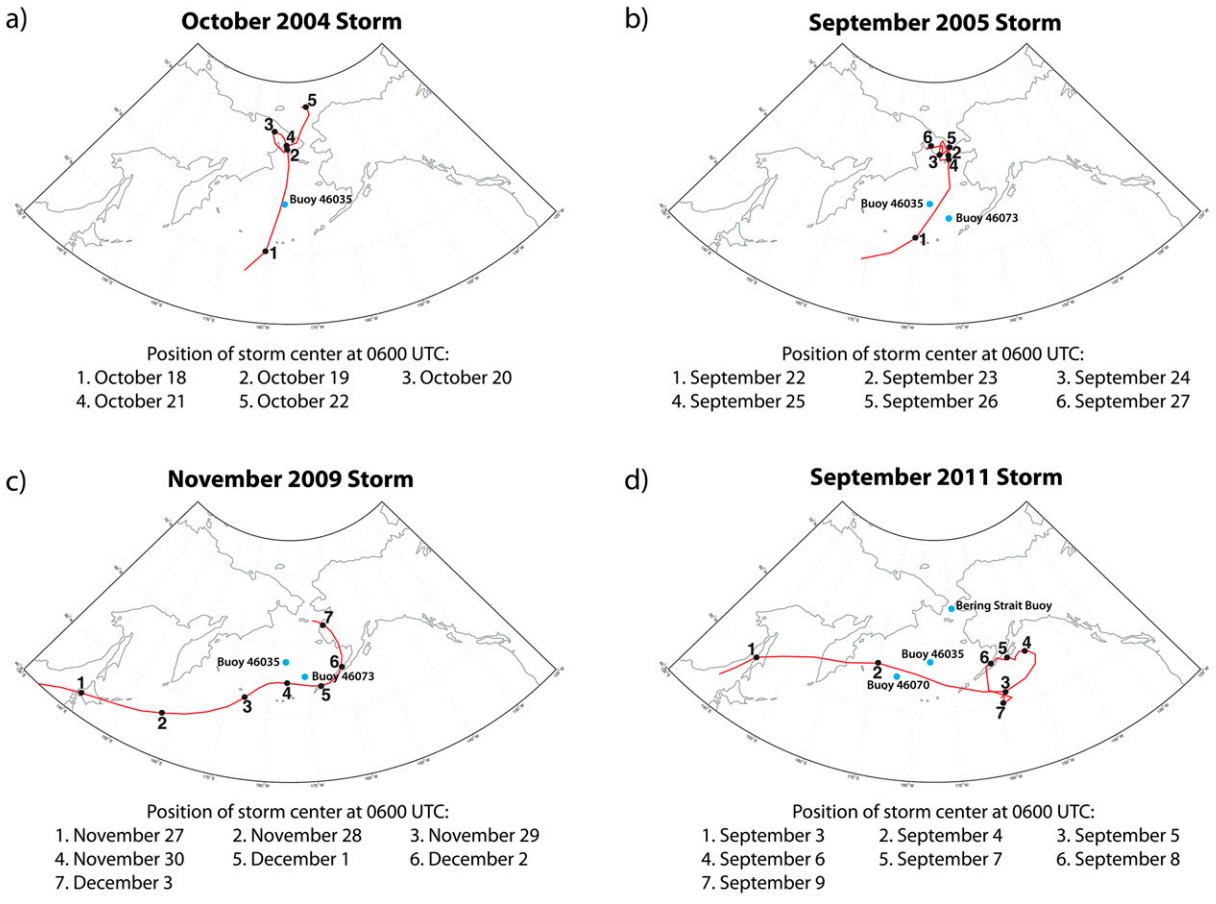

FIG. 2. Tracks of selected storms: (a) October 2004 storm, (b) September 2005 storm, (c) November 2009 storm, and (d) September 2011 storm. Location of buoys with data available during each storm event is also indicated.

resulting damage along the coasts of Norton Sound and the southern Chukchi Sea was estimated at roughly $2 million. Regional damage included coastal flooding, up to 9.1 m of localized beach erosion, minor structural damage to residential and commercial buildings, and roadway and airstrip washout (NCDC 1999).

c. *November 2009 storm*

A low pressure system (S09) moved east-northeast over the southern Bering Sea from 29 November to 2 December 2009 (Fig. 2c; note Alaska standard time is −0900 UTC). The storm reached peak strength on 30 November with a central pressure of approximately 960 hPa and was centered over the south-central Bering Sea. The storm system continued to move eastward, tracking along the Aleutian Islands and reaching the Alaska Peninsula on 2 December. In this study, storm dates are considered to be 27 November–4 December 2009, bracketing the storm peak strength and impact on the southern Bering Sea. The storm produced high winds up to 36 m s^{-1} with peak gusts around 45 m s^{-1}. The associated high surf resulted in coastal flooding across the Aleutian Islands and the Alaska Peninsula. The storm also produced heavy snow and blizzard conditions across the Bering Sea coastal region (NCDC 1999). Damage estimates were not calculated by the National Weather Service for this storm.

d. *September 2011 storm*

A low pressure system (S11) moved into and then loitered over the northwestern Gulf of Alaska–Alaska Peninsula region on 5–8 September 2011 (Fig. 2d). The storm reached peak strength early on 6 September with a minimum reported central pressure of 955 hPa while centered over the northwest quadrant of the Gulf of Alaska, just east of the Alaska Peninsula. As the system began to weaken, it continued to loiter, slowly meandering around the Alaska Peninsula region, for approximately 2 more days. On 9 September, as the storm system weakened further and moved southeastward over the Gulf of Alaska, a second system moved east over the Bering Strait–southern Chukchi Sea region from Russia, providing a secondary

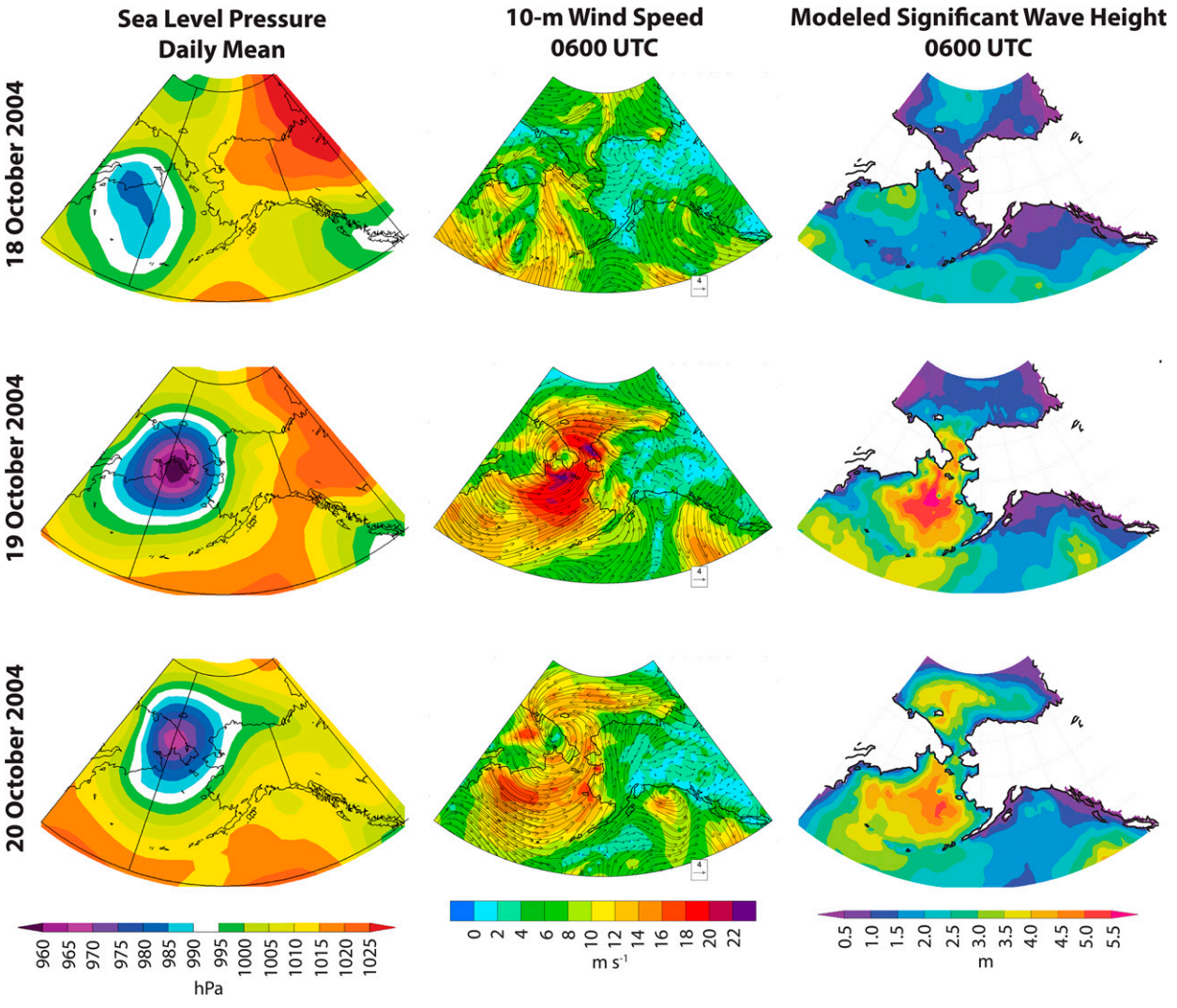

FIG. 3. Synoptic conditions and modeled wave states during the peak of the October 2004 storm: 18–20 Oct 2004. Mean sea level pressure plots created with NOAA's Earth System Research Laboratory, Physical Sciences Division, atmospheric variables plotting page (http://www.esrl.noaa.gov/psd/data/histdata/).

impact on the oceans to the west of Alaska. In this study, storm dates are considered to be 5–9 September 2011, covering the time from storm peak strength through its period of impact on the Bering Sea. The storm produced wind gusts up to 31 m s^{-1} along the Aleutian Islands and wind-wave heights up to 4.6 m within the Bering Sea. The National Weather Service did not perform impact and damage estimate reports for this event.

3. Global ocean wave model WAVEWATCH III

WAVEWATCH III, version 3.14 (WW3), is a full-spectral, third-generation wind-wave model developed at the Marine Modeling and Analysis Branch of the Environmental Modeling Center of NOAA's National Centers for Environmental Prediction. Governing equations within WW3 account for refraction of the wave field due to variations in mean water depth, wave growth and decay due to wind action, nonlinear resonant interactions, dissipation, bottom friction, and dynamically updated ice coverage. Similar to other spectral wave models, WW3 solves the linear balance equation for the spectral wave action density in terms of wavenumber and wave direction as a slowly varying function of space and time using the assumption that the space and time scales of individual waves are significantly smaller than the associated scale of change of the wave spectrum and of the mean depth and current (Tolman et al. 2002, p. 313). Within WW3, equations for spatial propagation, intraspectral propagation, and source terms are also solved consecutively at each global model time step (Tolman 2009). The spatial and

TABLE 2. Regional winds and modeled wave states during the peak of the October 2004 storm. (a) Sustained 10-m winds (direction, speed; m s^{-1}); (b) Hs (m); (c) Peak Hs (m) and location.

Time		Bering Sea	Bering Strait	Chukchi Sea
0600 UTC 18 Oct 2004	(a) Sustained 10-m winds (direction, speed; m s^{-1})	Southerly/southeasterly, 12–14	Easterly, 6–8	Southerly/southeasterly, 6–10
	(b) Hs (m)	2–3	0.5–1	0.5–1.5
	(c) Peak Hs and location (m)	3–3.5 in north-central Bering Sea	—	—
0600 UTC 19 Oct 2004	(a) Sustained 10-m winds (direction, speed; m s^{-1})	Westerly/southwesterly, 18–20	Southerly, 20–24	Easterly, 14–18
	(b) Hs (m)	4	3.5–5	3.5–5
	(c) Peak Hs and location (m)	5–7 in north-central Bering Sea	—	—
0600 UTC 20 Oct 2004	(a) Sustained 10-m winds (direction, speed; m s^{-1})	Westerly, 12–20	Southerly, 12–16	Southerly, 12–16
	(b) Hs (m)	3–4.5	3	3–4.5
	(c) Peak Hs and location (m)	4.5–5 in eastern Bering Sea	—	—

intraspectral propagation equations, the third-order-accurate ''ULTIMATE QUICKEST'' scheme of Leonard (1991; Tolman 2009), is used, which removes the ''garden sprinkler effect'' (Tolman 2002, 2009) from results (Tolman et al. 2002). WW3 source terms are wind input (speed and direction linearly interpolated during model runs), nonlinear interactions, whitecapping dissipation, and bottom friction; these are incorporated into the model using a modified version of the Wave Model (WAM) methodology (Tolman et al. 2002). WW3 can also incorporate currents and water levels. Sea ice concentrations are also included and can be treated either using a discontinuous method or a user-defined continuous method (Tolman et al. 2002; Tolman 2003). For more detailed descriptions of WW3, please see Tolman et al. (2002) and Tolman (2009).

In this study, WW3 is run in a mosaic, or multigrid, approach in which two grids with different resolutions are treated as a single wave model utilizing two-way nesting. This two-way nesting mosaic approach allows WW3 to provide increased local spatial resolution as the model simultaneously and continuously considers interaction between the grids, providing realistic boundary conditions for regions of interest (Tolman 2008). WW3 runs are completed using a lower-resolution Pacific basin grid with a nested, higher-resolution Alaskan grid (Fig. 1b). WW3 grid resolution for the Pacific basin grid is 1° × 1° and the grid resolution for the Alaskan region is 0.25° latitude × 0.50° longitude. The 10-m wind and sea ice concentration input data used in the WW3 runs are obtained from the National Weather Service's Global Forecast System (GFS) with 1° × 1° resolution and are updated at 6- and 24-h time intervals, respectively (data were obtained via NOAA's National Operational Model Archive and Distribution System). GFS winds were selected to drive WW3 in this study to be consistent with the operational use of WW3. A user-defined continuous sea ice treatment using a simple linear decay model is applied within WW3 to represent ice-induced attenuation of wave energy (Tolman 2003). For this study, critical sea ice concentrations at which obstruction begins and are complete are set at 25% and 75%, respectively. This means that grid points with sea ice concentrations less than 25% are considered ice free, and ice-induced wave attenuation is neglected, while grid points with sea ice concentrations greater than 75% are treated as solid sea ice (i.e., land) with no wave energy transmitted. At grid points with sea ice concentrations between 25% and 75%, the simple linear decay model is applied, providing ice-induced attenuation of wave energy with all wave energy dissipated by 75%. Model runs begin with calm ocean conditions and a 10–15-day spinup is necessary to develop realistic wave heights leading into and during storm event dates. Model runs completed in the study are building off of the model configuration (e.g., tuning values) previously determined for the Alaskan region by the Marine Modeling and Analysis Branch of NOAA's NCEP (Tolman 2008; Spindler and Tolman 2010).

4. Bering Sea and Bering Strait buoys

In situ data from four buoys provided information about wave parameters during the selected storms and enabled examination of WW3 significant wave height (Hs) performance at high temporal resolution. All buoys are located in the Bering Sea. Three are positioned off the continental shelf in deep water: 46070 (southwest Bering Sea; 55.083°N, 175.270°E; water depth of 3804 m), 46035 (central Bering Sea; 57.067°N, 177.750°W; water depth of 3658 m), and 46073 (southeast Bering Sea; 55.011°N, 171.981°W; water depth of 3051.5 m) (Fig. 1a).

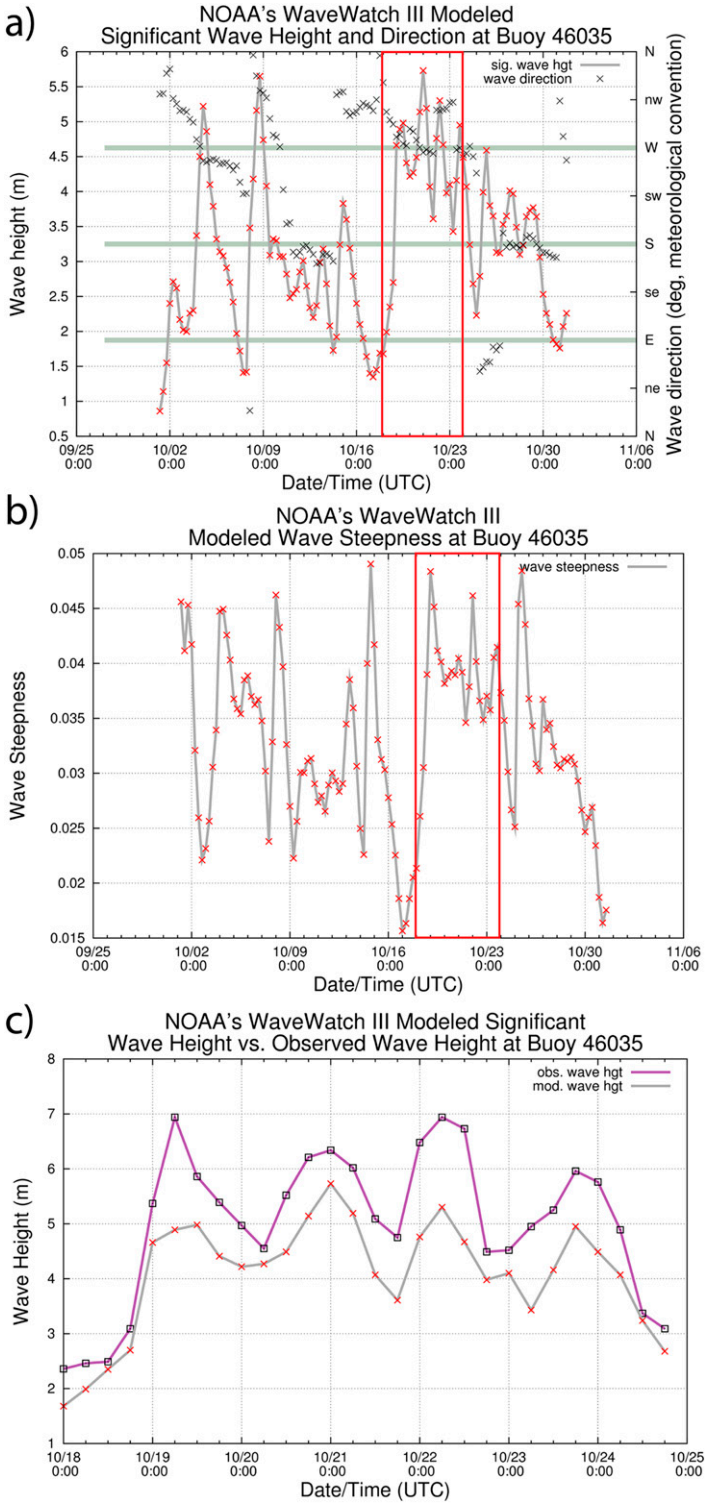

FIG. 4. Modeled (a) Hs and wave direction and (b) wave steepness at buoy 46035; October 2004 storm dates highlighted. (c) Modeled wave heights (gray) vs observed wave heights (purple) at buoy 46035 for the October 2004 storm dates.

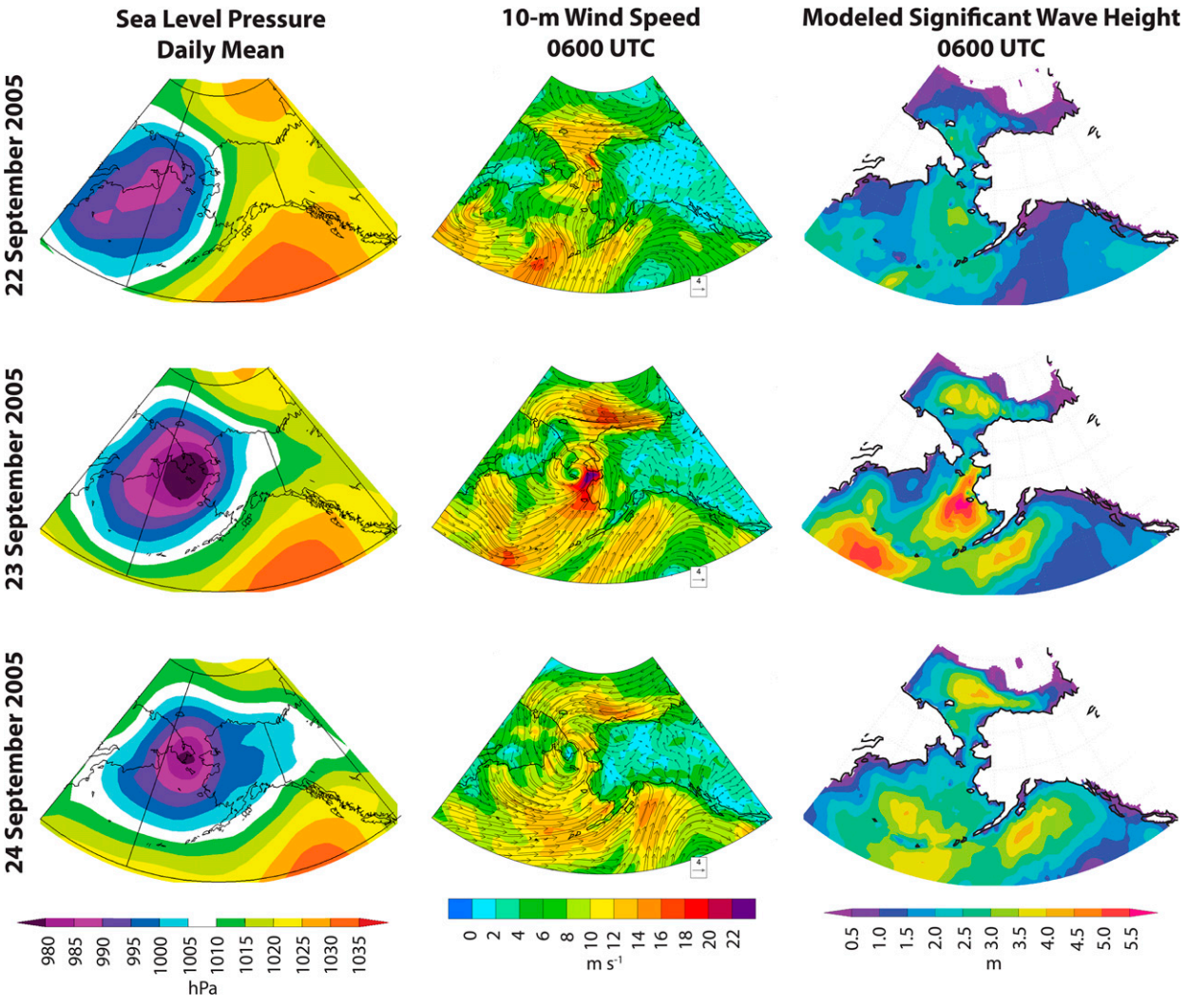

FIG. 5. Synoptic conditions and modeled wave states during the peak of the September 2005 storm: 22–24 Sep 2005. Note: Within the modeled wave-state plots, sea ice in the Arctic is represented in white. Mean sea level pressure plots created with NOAA's Earth System Research Laboratory, Physical Sciences Division, Atmospheric variables plotting page (http://www.esrl.noaa.gov/psd/data/histdata/).

Additional data are provided by a ''Watchmate'' buoy deployed temporarily in the shallow continental shelf waters just south of the Bering Strait (65.000°N, 168.750°W; water depth of ~50 m) 15 July–15 October 2011. This buoy, referred to as the ''Bering Strait buoy'' in this paper, was sponsored by the U.S. Environmental Protection Agency and NOAA and was procured from Axys Technologies.

5. Results

a. October 2004 storm

As S04 moved north over the central Aleutian Islands into the Bering Sea on 17–18 October (Fig. 2a), 10-m winds over the Bering Sea rapidly strengthened, influencing the regional wave state (Fig. 3; Table 2). WW3-modeled significant wave heights (Hs) also rapidly increased across the Bering Sea as the storm continued to strengthen and entered the Gulf of Anadyr region. By 0600 UTC 19 October, the storm system had strengthened to 941 hPa and was centered over the Gulf of Anadyr. At the storm peak (0600–1200 UTC 19 October), modeled Hs exceeded 4 m over much of the Bering Sea, with a peak Hs of 5–7 m in the north-central Bering Sea associated with the strongest wind speeds. Within the southern Chukchi Sea and Bering Strait, modeled Hs ranged between 3.5 and 5 m during the peak of the storm. Following the peak, the storm took up a quasi-stationary position over the Gulf of Anadyr–Chukotka

TABLE 3. Regional winds and modeled wave states during the peak of the September 2005 Storm. Note: Locations of the highest sustained 10-m winds and Hs are indicated in parentheses. (a) Sustained 10-m winds (direction, speed; m s^{-1}); (b) Hs (m); (c) Peak Hs (m) and location.

Time		Bering Sea	Norton Sound	Bering Strait	Chukchi Sea
0600 UTC 22 Sep 2005	(a) Sustained 10-m winds (direction, speed; m s^{-1})	Southerly, 8–14 (eastern Bering Sea)	Southerly, 12–16	Southerly shifting to easterly with increasing latitude, 10–12	Easterly, 10–16
	(b) Hs (m)	2–3.5 (eastern Bering Sea)	1.5–2.5	1.5–2.5	2–3
	(c) Peak Hs and location (m)	3.5–4 in the eastern Bering Sea	—	—	—
0600 UTC 23 Sep 2005	(a) Sustained 10-m winds (direction, speed; m s^{-1})	Southwesterly, 10–18 (eastern and western Bering Sea)	Southerly, 20–24	Easterly, 10–14	Easterly, 10–14
	(b) Hs (m)	4–6 (eastern Bering Sea)	2.5–3.5	2–2.5	2–2.5
	(c) Peak Hs and location (m)	6+ in the eastern Bering Sea	—	—	—
0600 UTC 24 Sep 2005	(a) Sustained 10-m winds (direction, speed; m s^{-1})	Westerly, 10–14 (central and eastern Bering Sea)	Southerly, 12–14	Southeasterly, 10–14	Easterly, 8–14
	(b) Hs (m)	2.5–3.5	1.5–2.5	2–2.5	2.5–3.5
	(c) Peak Hs and location (m)	3.5–4.5 in the southern Bering Sea	—	—	—

Peninsula region for the next few days and began to slowly weaken. During this period Hs also slowly declined. In addition to the large Hs, the modeled waves are also characterized by notable steepness, associated in particular with the largest wave heights (Figs. 4a,b).

Observed wave heights are only available from 46035 during this event (Fig. 1a). During the modeled period (18–24 October), WW3 underestimates observed Hs by approximately 0.5–1 m (Fig. 4c), although it accurately captures the timing of wave onset and decline. Larger discrepancies were noted during the periods of wave height peaks (19 and 22 October) with WW3 underestimating Hs by 1.5–2 m.

b. *September 2005 storm*

As S05 moved north over the east-central Bering Sea on 22 September (Fig. 2b) and continued to intensify, southerly 10-m winds over the Bering Sea strengthened, with the strongest sustained winds observed over the eastern Bering Sea, including Norton Sound (Fig. 5; Table 3). At the storm peak (0600 UTC 23 September), WW3 generated Hs of 4–6 m in the eastern Bering Sea, 2.5–3.5 m in Norton Sound, and 2–2.5 m in the Chukchi Sea. The storm system then stalled, loitering over the northern Bering Sea–Bering Strait region for the next 3 days, promoting the continuation of large wind waves in the Bering and Chukchi Seas. In addition to the large Hs produced by this storm system, the wind waves generated by WW3 are also characterized by notable steepness, particularly during periods of wave height peaks (Fig. 6, top and middle). Similar to S04, rapid initial storm motion followed by a period of loitering meant rapid Hs magnitude onset followed by a slow decline.

During S05, observed wave heights are available from 46035 and 46073 (Fig. 1a). Similar to S04, WW3 primarily underestimates Hs (Fig. 6, bottom) during the event on the order of 0.5 m or less at both buoy locations while accurately capturing the timing of wave onset, peak, and decline. WW3 again considerably underestimates Hs during peak wave heights, with discrepancies of approximately 1–1.5 m.

c. *November 2009 storm*

As S09 moved east-northeastward, toward the western Aleutian Islands on 29 November (Fig. 2c), it began to influence the extreme southwesterly Bering Sea region (Fig. 7; Table 4). As the system continued to slowly move, following the Aleutian Island chain, 10-m wind speeds increased over the southwesterly and south-central Bering Sea regions. Over a 12-h period (0000–1200 UTC 29 November), sustained wind speeds across the central southern Bering Sea strengthened significantly with localized wind speed increases of up to ~15 m s^{-1}; modeled Hs rapidly increased in response. At the storm peak (1800 UTC 29 November–0000 UTC 30 November), modeled Hs exceeded 6 m across much of the southern Bering Sea, with peak heights of 9–10 m in the southwest Bering Sea, and Hs as large as 12 m in the eastern North Pacific. Following the storm peak, the system continued to track easterly along the Aleutian Islands, with the center shifting just south of the Aleutians. Weakening was gradual, and strong sustained winds continued to persist, with modeled Hs exceeding 6 m over much of the Bering Sea. In addition to the large Hs, modeled wind waves are also characterized by notable steepness, especially during the storm peak (Fig. 8, top and middle). Unlike S04 and

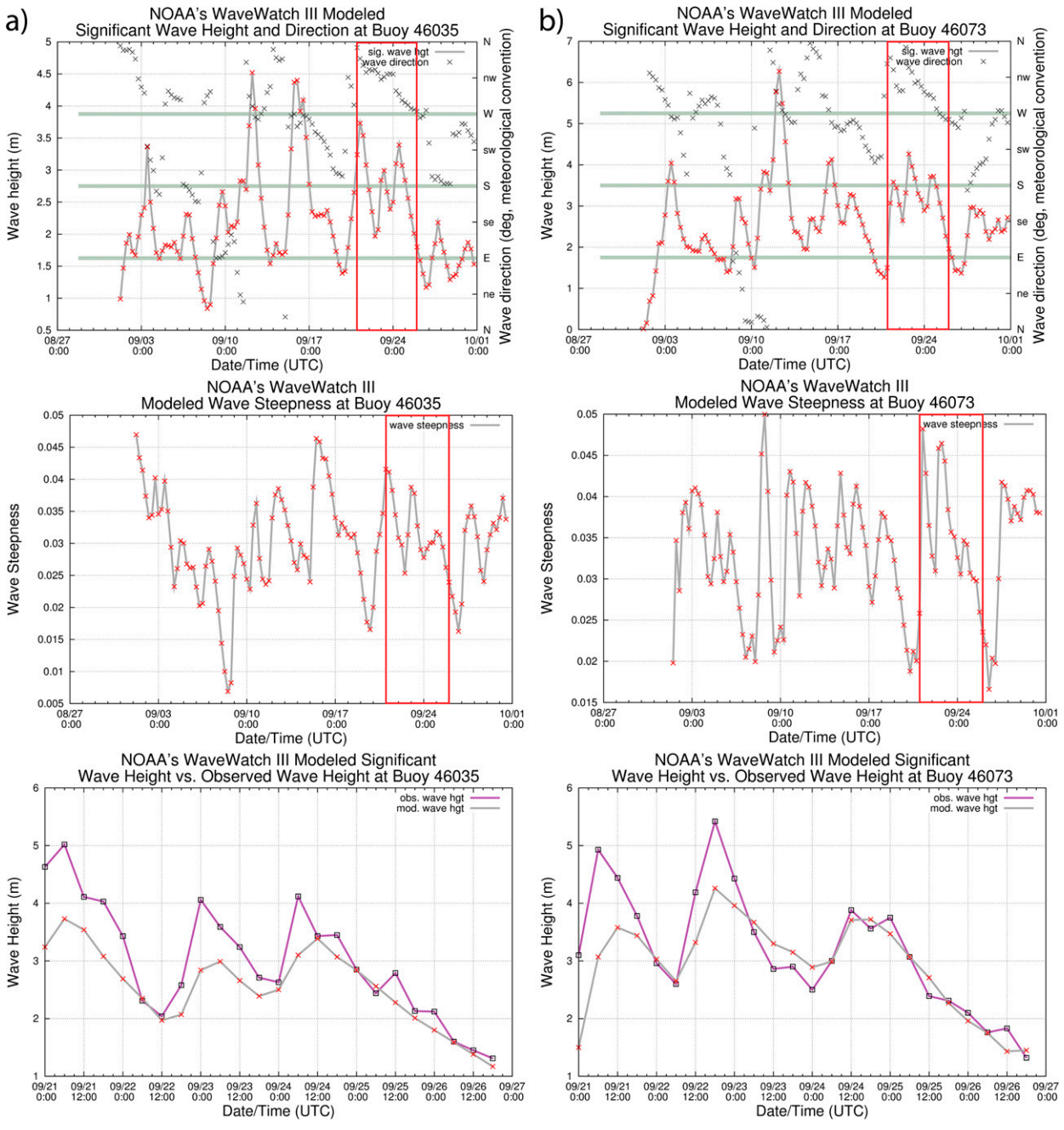

FIG. 6. Modeled (top) Hs and wave direction and (middle) wave steepness at (a) buoy 46035 and (b) buoy 46073; September 2005 storm dates highlighted. (bottom) Modeled wave heights (gray) vs observed wave heights (purple) at (a) buoy 46035 and (b) buoy 46073 for the September 2005 storm dates.

S05, this storm did not loiter, which resulted in a rapid onset and a relatively rapid decline of Hs in the Bering Sea.

During S09 observed wave heights are available from 46073 and from 46035 during the first part of the storm (Fig. 1a). At 46073 WW3, in general, accurately captures observed Hs magnitude, exhibiting both over- and underestimation of less than 0.5 m, and timing of wave onset, growth, and decline (Fig. 8a, bottom). WW3 underestimates Hs prior to the storm peak (30 November) while overestimating Hs as the storm subsequently weakens and moves away from the buoy location. During the storm peak (0000 and 1800 UTC 30 November), however, large discrepancies are noted: WW3

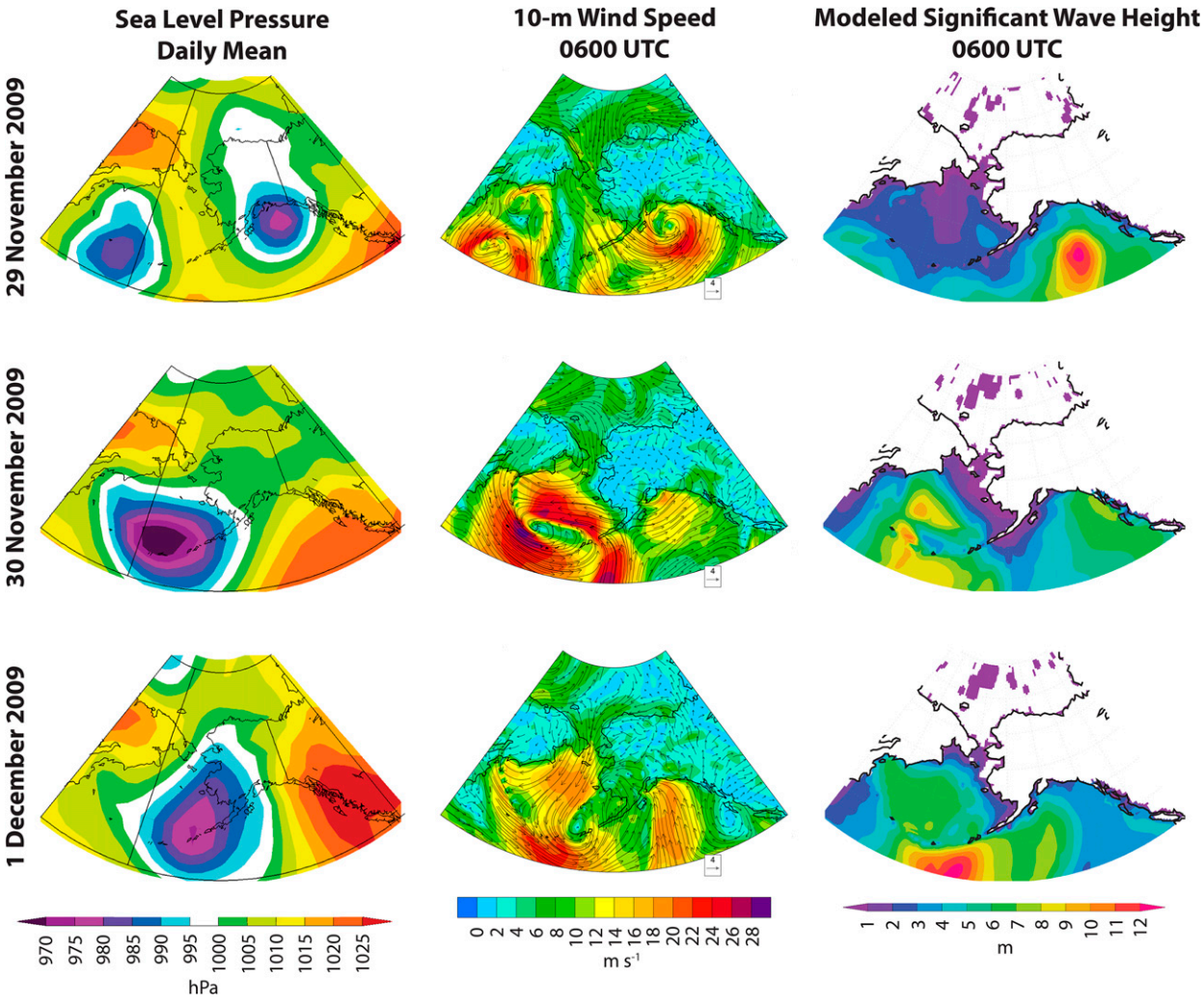

FIG. 7. Synoptic conditions and modeled wave states during the peak of the November 2009 storm: 29 Nov–1 Dec 2009. Note: Within the modeled wave-state plots, sea ice in the Arctic is represented in white. Mean sea level pressure plots created with NOAA's Earth System Research Laboratory, Physical Sciences Division, atmospheric variables plotting page (http://www.esrl.noaa.gov/psd/data/histdata/).

underestimates Hs at the primary peak (0000 UTC) by nearly 2 m but then overestimates the secondary peak (1800 UTC) by approximately 1 m. At 46035, WW3 again captures observed Hs magnitude and timing of wave onset and growth prior to the storm peak, with overall Hs discrepancies of less than 0.5 m (Fig. 8b, bottom). Near the time of the storm peak, however, WW3 begins to considerably underestimate Hs with discrepancies of approximately 1 and 2 m during the onset (0600–1800 UTC 29 November) and peak of the storm (0000–1200 UTC 30 November), respectively.

d. September 2011 storm

As S11 strengthened and slowed to loiter over the northwestern Gulf of Alaska–Alaska Peninsula region on 5 September (Fig. 2d), northerly winds over the Bering Sea, Bering Strait, and Chukchi Sea began to strengthen and WW3-modeled Hs began to increase (Fig. 9; Table 5). At the storm peak (0000–1200 UTC 6 September), WW3 generated Hs of 3–4 m over much of the Bering Sea with peak Hs of 4.5–5.5 m in the central Bering Sea, 3.5 m in the Bering Strait, and 3–3.5 m in the Chukchi Sea. Late on 6 September (1800 UTC 6 September–0000 UTC 7 September), the strongest sustained winds shifted from the central to the eastern Bering Sea while wind waves continued to grow in both regions. Early on 7 September, WW3-modeled Hs in the eastern Bering Sea were approximately 4–6 m with peak Hs in the southeast Bering Sea exceeding 6 m. Although the storm system weakened following 6 September, strong winds and large wind waves continued to influence the Alaskan region as the system continued to

TABLE 4. Regional winds and modeled wave states during the peak of the November 2009 Storm. Note: Locations of the highest sustained 10-m winds are indicated in parentheses. (a) Sustained 10-m winds (direction, speed; m s^{-1}); (b) Hs (m); (c) Peak Hs (m) and location.

Time		Bering Sea	Extreme North Pacific
0600 UTC 29 Nov 2009	(a) Sustained 10-m winds (direction, speed; m s^{-1})	Northerly, 8–14 (eastern Bering Sea); Southerly, 8–16 (western Bering Sea)	Counterclockwise rotation around the storm center, 12–24 (western extreme North Pacific)
	(b) Hs (m)	1–3	3–5
	(c) Peak Hs and location (m)	3–4 in southern Bering Sea	5–6 in western extreme North Pacific
0600 UTC 30 Nov 2009	(a) Sustained 10-m winds (direction, speed; m s^{-1})	Easterly, 20–28	Westerly, 20–30
	(b) Hs (m)	4–9	4–9
	(c) Peak Hs and location (m)	9–10 in west-central Bering Sea	9–10 in west-central Bering Sea
0600 UTC 1 Dec 2009	(a) Sustained 10-m winds (direction, speed; m s^{-1})	Northerly/northeasterly, 14–20	Westerly, 20–24
	(b) Hs (m)	6–7	7–12
	(c) Peak Hs and location (m)	7–8 in south-central Bering Sea	12+ in east-central Bering Sea

loiter over the Alaska Peninsula for another 2 days. In addition to the large Hs, modeled wind waves are steep, particularly when peak wave heights are generated (Fig. 10, top and middle). For all affected regions, during the period of storm strengthening, there is a rapid onset of large, steep wind waves throughout the Alaskan region. The rate of decline of these wind waves, however, is dependent on proximity to the storm system as it meanders around the Alaska Peninsula region: Hs declines rapidly at locations closer to the storm center (e.g., buoy stations 46035 and 46070; Figs. 10a,b, top and middle), whereas at locations farther away (e.g., Bering Strait buoy; Fig. 10c, top and middle), the decline is less rapid. When the storm finally moves away from the Alaska Peninsula region (8–9 September), Hs in the northern Bering Sea and Bering Strait experiences a rapid decline.

During S11, observed wave heights are available from 46035 and 46070, and from the Bering Strait buoy (Fig. 1a). At both 46035 and 46070 WW3 accurately captures Hs magnitudes, with wave height discrepancies of 0.5 m or less, as well as timings of wave onset, growth, and decline (Figs. 10a,b, bottom). In general, at 46035, WW3 overestimates Hs by up to ~0.5 m during the peak of the storm (0000 UTC 6 September–0000 UTC 7 September) (Fig. 10a, bottom). However, Hs discrepancies of only 0.1–0.3 m are observed during the onset and decline of the large wind waves. At 46070, however, WW3 primarily underestimates Hs (Fig. 10b, bottom). Within the southwest Bering Sea (e.g., 46070), peak Hs was observed on 5 September, prior to the storm peak and the subsequent easterly shift in peak sustained winds from the central to eastern Bering Sea. WW3 underestimates Hs during this local peak in wind waves by 0.4–0.7 m at 46070. Similar discrepancies are also observed during a secondary peak in wind waves on 9 September, which is associated with a new storm system moving easterly over the Bering Strait–southern Chukchi Sea region from Russia. During the remainder of S11, though, WW3-modeled Hs at 46070 are accurately captured with discrepancies of 0.5 m or less. At the Bering Strait buoy, however, WW3 exhibited larger Hs magnitude underestimations (Fig. 10c, bottom). Between 0000 UTC 5 September and 0600 UTC 7 September, WW3 underestimates Hs by approximately 1–1.5 m, with the largest discrepancies observed during the peak of the storm (1800 UTC 5 September–1200 UTC 6 September). Similar to 46070, large discrepancies are also observed at the Bering Strait buoy at 1200–1800 UTC 9 September as the new storm system moves into the region from Russia. During the decline in wind waves associated with S11 (1200 UTC 7 September–0600 UTC 9 September), though, Hs discrepancies are 0.5 m or less at the Bering Strait buoy. WW3 accurately modeled the timing of wave onset, growth, and decline at the Bering Strait buoy.

6. Discussion and conclusions

Storm systems positioned over the northern Bering Sea, Bering Strait, and southern Chukchi Sea region, such as the S04 and S05 events, were positioned to generally produce westerly/southwesterly winds over the Bering Sea and easterly winds over the Chukchi Sea. Strong winds associated with these storms can also be persistent because these storms often stall; this results in the potential to produce sustained periods of large, often steep, wind waves in the ocean west of Alaska. At the storm peak for S04 and S05, sustained 10-m winds up to 20 m s^{-1} were observed over the Bering Sea and 24 m s^{-1}

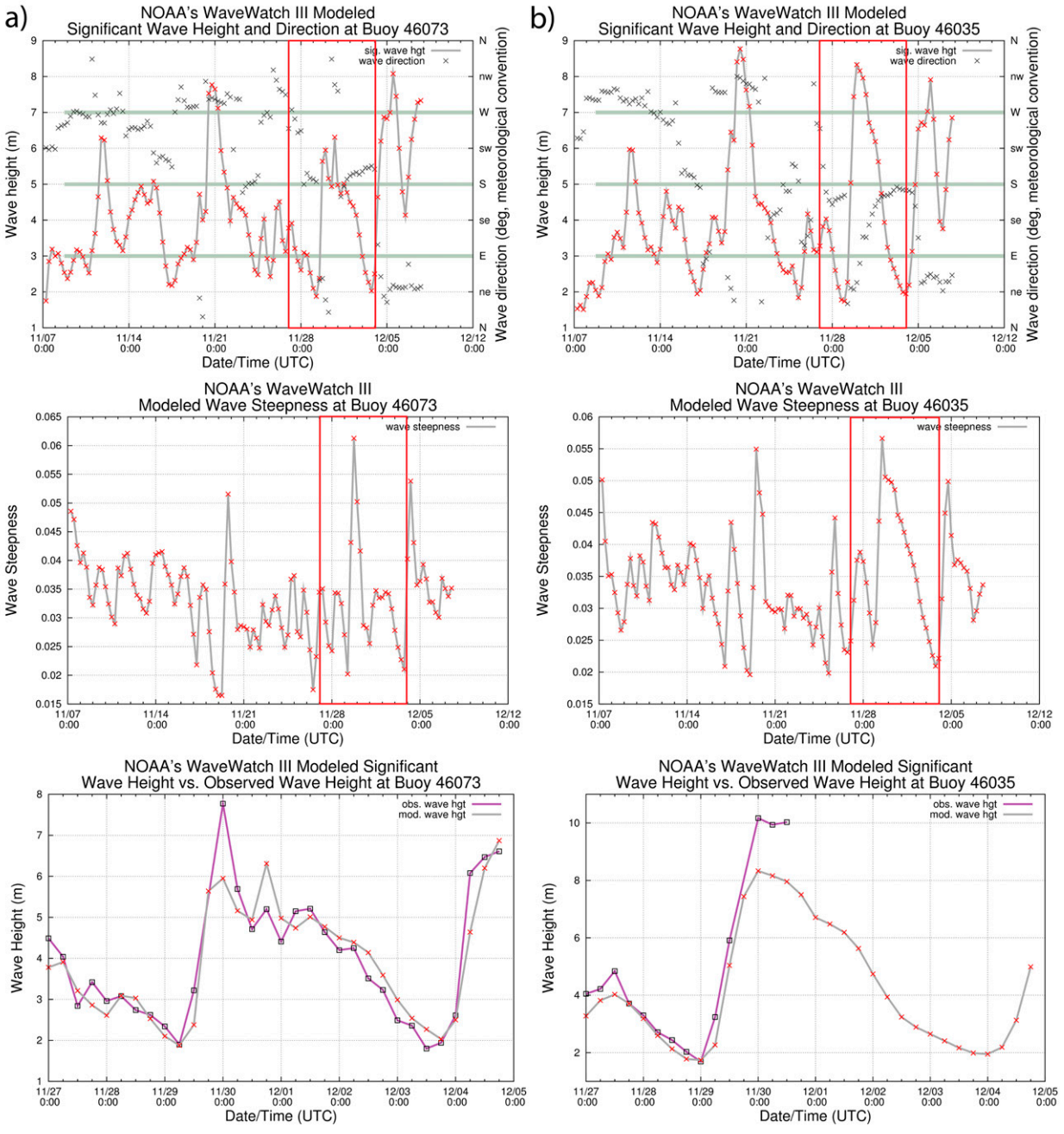

FIG. 8. Modeled (top) Hs and wave direction and (middle) wave steepness at (a) buoy 46073 and (b) buoy 46035; November 2009 storm dates highlighted. (bottom) Modeled wave heights (gray) vs observed wave heights (purple) at (a) buoy 46073 and (b) buoy 46035 for the November 2009 storm dates.

over the Bering Strait and Chukchi Sea. While at peak strengths and positioned west of the Seward Peninsula, these storms generated WW3-modeled Hs as high as 7 m in the Bering Sea and 5 m in the Bering Strait and Chukchi Sea. Storm systems that approach the northern Bering Strait–southern Chukchi Sea region rapidly and then loiter over the ocean, such as S04 and S05, also exhibit a rapid development and a slow decline of wind waves. This wave-state response is typical of stalled systems and is well captured by WW3 during both events (Figs. 4a,b and 6, top and middle). While wind waves in general exhibited large steepness values throughout the S04 and S05 events, steepness decreased noticeably during periods when the storm systems were stalled.

Storm systems positioned over or just north of the Aleutian Islands, such as the S09 event, generally

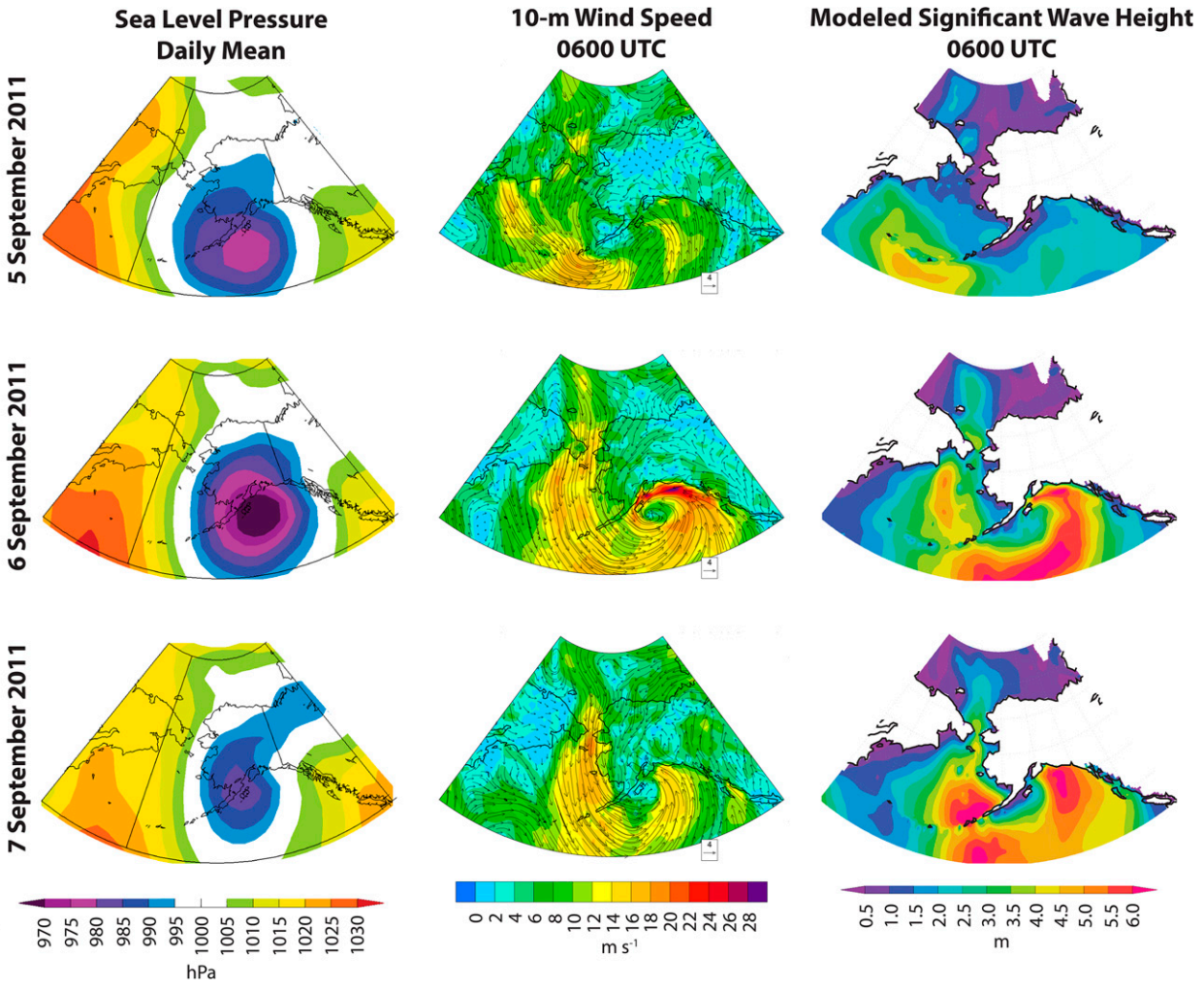

FIG. 9. Synoptic conditions and modeled wave states during the peak of the September 2011 storm: 5–7 Sep 2011. Note: Within the modeled wave-state plots, sea ice in the Arctic is represented in white. Mean sea level pressure plots created with NOAA's Earth System Research Laboratory, Physical Sciences Division, atmospheric variables plotting page (http://www.esrl.noaa.gov/psd/data/histdata/).

produce easterly winds over much of the Bering Sea and westerly winds impacting the Aleutians (and extreme North Pacific). Strong sustained winds associated with these types of severe storms have the potential to produce large, steep wind waves in the Bering Sea with maximum significant wave heights affecting the southern Bering Sea and Aleutian Islands. At its peak, S09 generated sustained winds up to 30 m s^{-1} over much of the southern Bering Sea and modeled Hs exceeded 6 m across much of the southern Bering Sea, with maximum Hs as high as 10 m in the southwest Bering Sea. Storm systems that do not stall or loiter, such as S09, exhibit a rapid onset but also a relatively rapid decline of large wind waves (Fig. 8, top and middle). These wind waves also maintain consistently large values for steepness due to the continued storm movement. The S09 storm peak is also clearly visible as maxima in both the Hs and steepness plots.

Storm systems positioned over the Alaska Peninsula, such as the S11 event, generally produce northerly winds over the Bering Sea, Bering Strait, and Chukchi Sea, impacting all of the ocean west of Alaska. Strong winds associated with these types of storm events have the potential to produce large, steep wind waves throughout the ocean west of Alaska, with maximum Hs generally observed in the Bering Sea. At the storm peak of S11, sustained winds up to 18 m s^{-1} were observed over the Bering Sea and Bering Strait and 16 m s^{-1} over the Chukchi Sea. At peak strength and positioned over the Alaska Peninsula, S11 modeled Hs exceeded 5–6 m in the central and eastern Bering Sea, and 3.5–4 m in the Bering Strait and Chukchi Sea. Although this type of storm system loiters, the positioning and meandering of its center over the Alaska Peninsula region, such as during the S11 event, causes the region of maximum

TABLE 5. Regional winds and modeled wave states during the peak of the September 2011 Storm. Note: Locations of highest sustained 10-m winds and significant wave heights are indicated in parentheses. (a) Sustained 10-m winds (direction, speed; m s^{-1}); (b) Hs (m); (c) Peak Hs (m) and location.

Time		Bering Sea	Bering Strait	Chukchi Sea
0600 UTC 5 Sep 2011	(a) Sustained 10-m winds (direction, speed; m s^{-1})	Northerly, 8–10 m s^{-1}	Northerly, ~8 m s^{-1}	Northerly, 6–10 m s^{-1}
	(b) Hs (m)	1.5–2.5	~0.5	0.5–2
	(c) Peak Hs and location (m)	3.5–4 in south-west Bering Sea	—	—
0600 UTC 6 Sep 2011	(a) Sustained 10-m winds (direction, speed; m s^{-1})	Northerly, 16–18 (central and eastern Bering Sea)	Northerly, 14–18	Northerly, 12–16
	(b) Hs (m)	3–4	3.5	3–3.5
	(c) Peak Hs and location (m)	4.5–5.5 in central Bering Sea	—	—
0600 UTC 7 Sep 2011	(a) Sustained 10-m winds (direction, speed; m s^{-1})	Northerly, 12–18 (eastern Bering Sea)	Northerly, 14–20	Northerly, 10–16
	(b) Hs (m)	4–6 (eastern Bering Sea)	3.5–4	2.5–4
	(c) Peak Hs and location (m)	6+ in south-east Bering Sea	—	—

sustained winds to shift over time and prevent the sort of persistence associated with a truly stalled storm. The resulting large, steep wind waves exhibit rapid onset and relatively rapid decline. The rate of decline of the large, steep wind waves, however, was noted to be a function of distance to the storm, with the rate of decline generally slowing with distance and latitude (Fig. 10, top and middle). For locations close to the storm center, the S11 storm peak is clearly visible as maxima in both the Hs and steepness plots. For locations farther from the storm system, large Hs and steepness maxima are also coincident with the storm peak but persist for approximately 48 h before declining. Nevertheless, these maximum Hs and steepness values are still noticeably larger than those values generated throughout the remainder of the event, particularly Hs values.

Of the four severe storm events analyzed in this study, S09 (third lowest minimum central pressure) produced the strongest sustained winds (easterlies of up to 30 m s^{-1}) and the largest, and the steepest, WW3-modeled Hs (9–10 m) within the Bering Sea. The storm event, however, only impacted the Bering Sea as the Chukchi Sea and the Bering Strait were covered with extensive sea ice. Of the storm events that impacted all of the ocean west of Alaska (S04, S05, and S11), S04 (lowest minimum central pressure) produced the strongest sustained winds and the largest modeled Hs across the region with 18–20 m s^{-1} winds and 5–7-m wind waves in the Bering Sea, 20–24 m s^{-1} winds and 3.5–5-m wind waves in the Bering Strait, and 14–18 m s^{-1} winds and 3.5–5-m wind waves in the Chukchi Sea. While WW3-modeled Hs varied between storm events and locations (Bering Sea, Bering Strait, and Chukchi Sea), maximum WW3 model wave steepness values at the buoy locations utilized were similar for the S04, S05, and S11 events. Nevertheless, all four storms are considered severe (Table 1) and produced strong 10-m winds and large, steep wind waves that significantly impacted western Alaska in various ways.

Overall, WW3 typically underestimates Hs for each storm event at all buoy locations utilized, although instances of overestimation were noted. In general, these underestimations are on the order of 0.5 m or less, representing an average underestimation of approximately 15%. Individual Hs underestimation percentages depend on buoy location with respect to the storm event, and range from approximately 8% (S04 at buoy 46035; Fig. 4c) to 33% (S11 at Bering Strait buoy; Fig. 10c, bottom). Larger discrepancies, however, are observed during periods of peak Hs. These discrepancies are on the order of 1–2 m, considerably underestimating the observed significant wave heights and representing an average underestimation of approximately 26%, with specific discrepancies ranging from 18% (S05 at buoy 46073; Fig. 6b, bottom) to 43% (S05 at buoy 46035; Fig. 6a, bottom). In general, the percentage of underestimation increases as the Hs discrepancy increases and is notably higher for the larger values of Hs during all the storm events. While the average 0.5 m or less WW3 underestimation percentages are approximately the same (16%–18%) for all three storm types (based on storm position), the larger underestimation (1–2 m) percentages are noted during the S04/S05 and S11 events when the storm systems were positioned over the Bering Strait and Alaska Peninsula regions, respectively, at 28% compared to 22% during S09 when the storm system was positioned over the Aleutian Islands. Discrepancies of Hs were noted irrespective of storm movement (stalled vs unstalled) during the S04 and S05 events. Unlike Hs, the timing and form of the observed wave

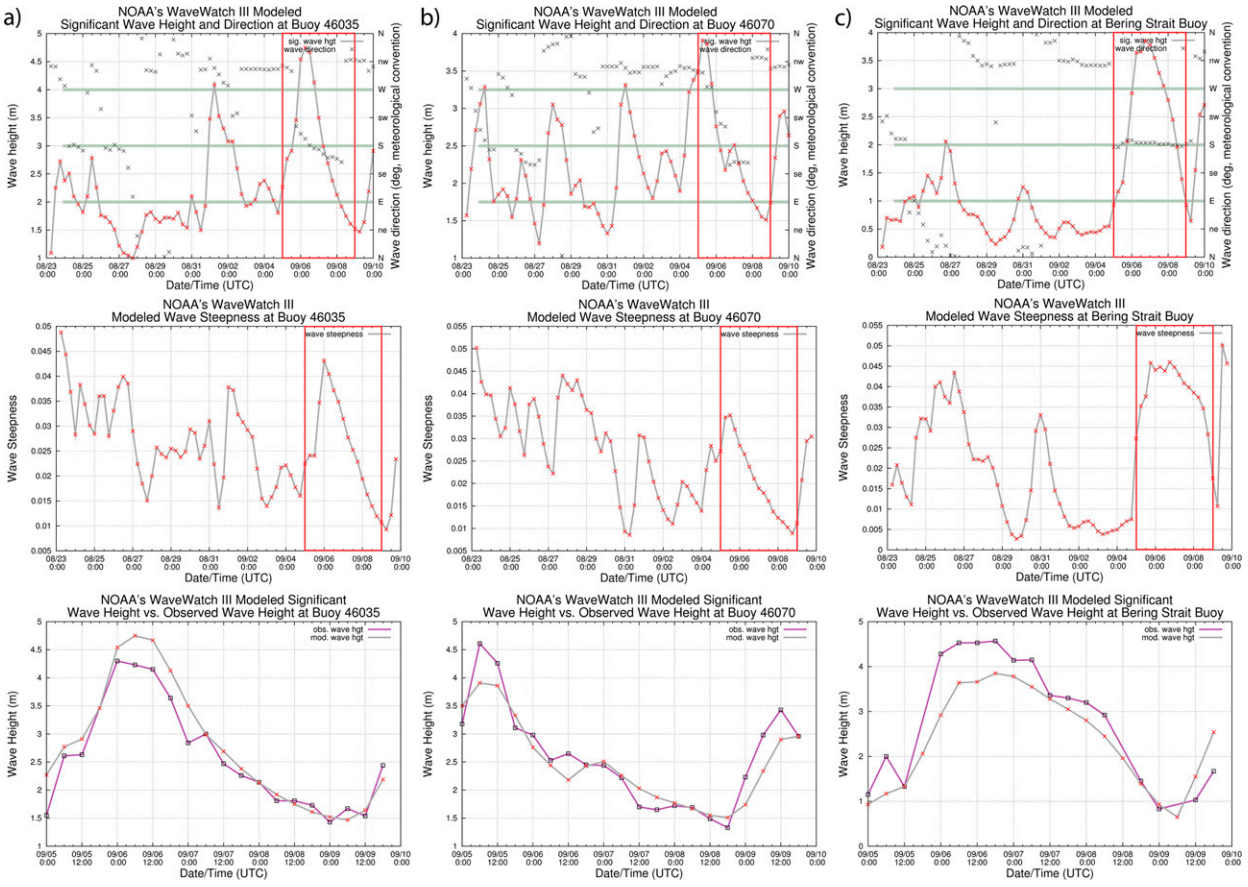

FIG. 10. Modeled (top) Hs and wave direction and (middle) wave steepness at (a) buoy 46035, (b) buoy 46070, and (c) Bering Strait buoy; September 2011 storm dates highlighted. (bottom) Modeled wave heights (gray) vs observed wave heights (purple) at (a) buoy 46035, (b) buoy 46070, and (c) Bering Strait buoy for the September 2011 storm dates.

action (onset, growth, peak, and decline of large, steep wind waves) is accurately captured by WW3 during all four severe storm events.

It should be noted that the skill of wave models such as WW3 is dependent on the accuracy of the forcing wind field; as well, the use of biased surface (e.g., 10 m) winds has been found to directly result in biases in the resulting modeled wave states (e.g., Hs) (Cardone et al. 1996; Rogers and Wittmann 2002; Durrant and Greenslade 2011, 2012; Durrant et al. 2013). For instance, underestimation of surface winds in gridded data products are known to result in underestimation of Hs (Durrant and Greenslade 2011, 2012; Durrant et al. 2013). Correction of the forcing wind field is found to improve accuracy of the modeled wave states throughout the extratropics, though localized underestimation of Hs continues to be present in the Bering and Chukchi Sea regions (Durrant et al. 2013, 2014). The GFS 10-m winds used in this study have not been corrected. GFS wind speeds were compared against the observed wind speeds at the buoy locations for the storm events (Fig. 11), and an overall agreement was found with general GFS wind speed underestimations on the order of $\sim 3\ \mathrm{m\ s^{-1}}$ or less. Notable discrepancies between the GFS and observed wind speed are found at the beginning and end of the September 2011 storm event at buoy 46070, during which the observed wind speeds are considerably lower than the GFS wind speeds. Large discrepancies are also found throughout the September 2011 storm at the Bering Strait buoy, during which GFS wind speeds are significantly higher than the observed wind speeds. This mismatch between the GFS and observed wind speeds for the Bering Strait buoy may be due to the smaller size of the buoy, however, as the buoy, with anemometers mounted at 2 and 2.5 m (compared to 5 m on the Bering Sea buoys), can be more easily dwarfed by larger waves, thus preventing the accurate recording of wind speeds during severe events. Nevertheless, the use of corrected winds could potentially improve the small magnitude but consistent underestimation of Hs found in this study (0.5 m or less, representative of an underestimation of Hs by ~15%); however, the larger

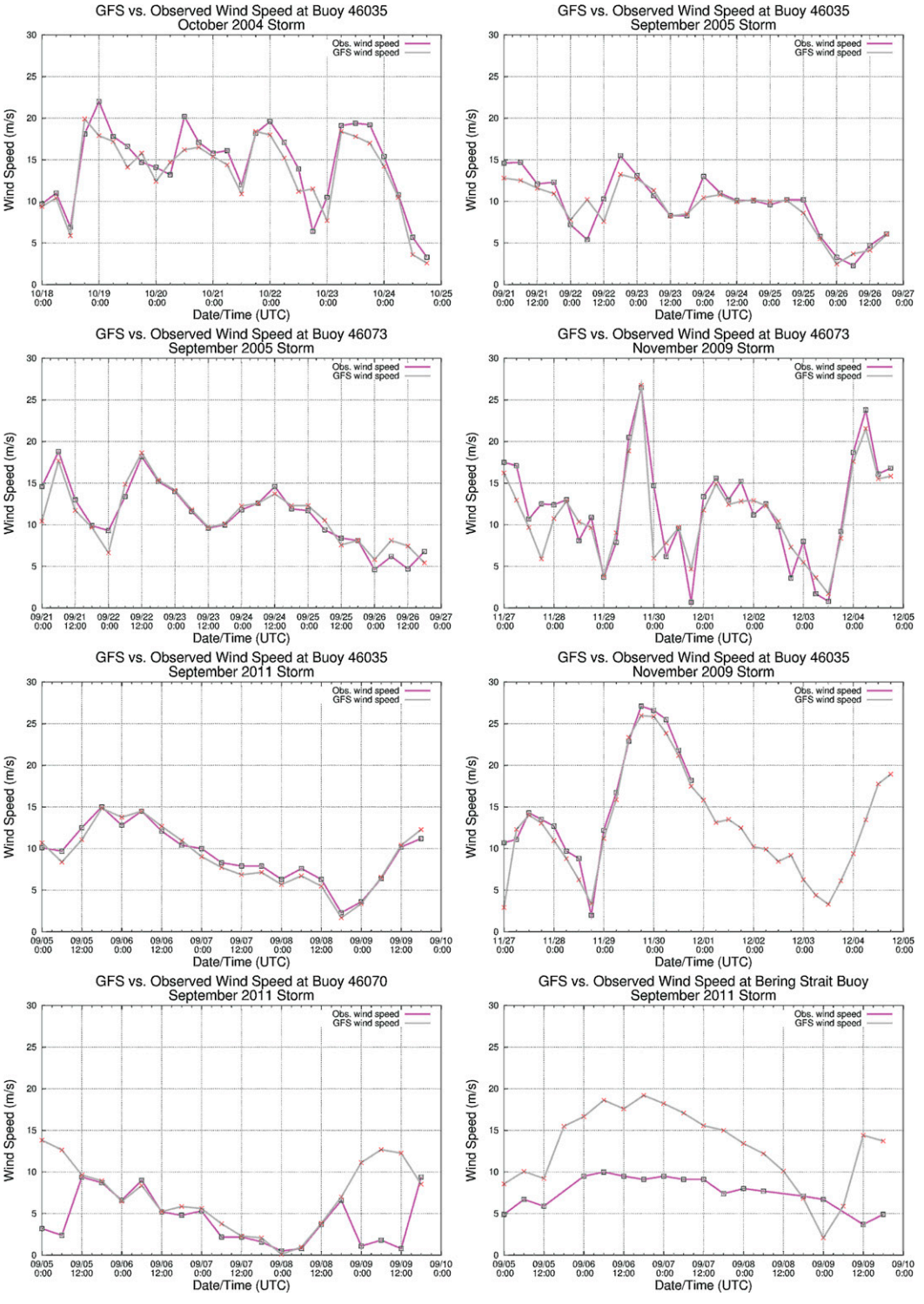

FIG. 11. GFS vs observed wind speeds at buoy locations utilized during each storm event.

discrepancies (1–2 m) observed during periods of peak Hs would likely persist.

The general Hs underestimations and discrepancy values observed in this study are comparable to those reported in Chawla et al. (2009, 2011). Chawla et al. (2009), using altimeter data, reported an overall negative bias in the southern Bering Sea with WW3 underestimating Hs by approximately 0.4 m or less. Chawla

et al. (2011), also using altimeter data for validation, reported an overall positive bias in the southern Bering Sea with WW3 overestimating Hs by approximately 0.4 m or less, a negative bias in the northern Bering Sea and Bering Strait, with WW3 underestimating Hs by approximately 0.5 m or less, and a positive bias in the Chukchi Sea with WW3 overestimating Hs by approximately 0.1 m or less. Chawla et al. (2009) also indicated that larger Hs biases were observed in the fall and winter months when more severe storms, such as those studied here, move through the Alaskan region. While there are differences in methodology between this study and the validation studies completed by Chawla et al. (2009, 2011), the similar overall underestimation bias and discrepancy values suggest that WW3 wave-state reconstructions are suitable for an event-level examination of resultant wind-wave states.

Acknowledgments. Funding for this research was provided by NOAA Grant NA09OAR4600220, "Social Vulnerability to Climate Change in the Alaskan Coastal Zone" under PI David Atkinson. Funding for the Bering Strait buoy was provided by EPA Grant IA 1392274 and NOAA Cooperative Institute for Arctic Research (CIFAR) Project 010-018 under PI David Atkinson. This research was also supported in part by a grant of HPC resources from the Arctic Region Supercomputing Center at the University of Alaska Fairbanks.

Thanks to Arun Chawla and the NCEP EMC Marine Modeling and Analysis Branch for help with interpreting WAVEWATCH III source code and preparing model run scripts. Thanks to Don Bahls, Oralee Hudson, and the Arctic Region Supercomputing Center for help compiling, running, and troubleshooting WAVEWATCH III on the ARSC Penguin Computing Cluster. Thanks to John Lingaas and the Fairbanks National Weather Service Office for providing poststorm assessments for the October 2004, September 2005, and November 2009 storms, and for providing help locating storm assessments for the November 2011 storm.

Additionally, thanks to the two anonymous reviewers, who provided valuable comments on an earlier version of this manuscript.

REFERENCES

Blier, W., S. Keefe, W. A. Shaffer, and S. C. Kim, 1996: Observational and numerical modeling investigations of three Bering Sea storms and their associated storm surges in the region of Nome, Alaska. Preprints, *First Conf. on Coastal Oceanic and Atmospheric Prediction*, Atlanta, GA, Amer. Meteor. Soc., 10.4. [Available online at http://www.nws.noaa.gov/mdl/pubs/Documents/Papers/Shaffer1998ObservationalAndNumerical.pdf.]

——, ——, ——, and ——, 1997: Storm surges in the region of western Alaska. *Mon. Wea. Rev.*, **125**, 3094–3108, doi:10.1175/1520-0493(1997)125<3094:SSITRO>2.0.CO;2.

Cardone, V. J., R. E. Jensen, D. T. Resio, V. R. Swail, and A. T. Cox, 1996: Evaluation of contemporary ocean wave models in rare extreme events: The "Halloween storm" of October 1991 and the "storm of the century" of March 1993. *J. Atmos. Oceanic Technol.*, **13**, 198–230, doi:10.1175/1520-0426(1996)013<0198:EOCOWM>2.0.CO;2.

Chawla, A., H. L. Tolman, J. L. Hanson, E.-M. Devaliere, and V. M. Gerald, 2009: Validation of a multi-grid WAVEWATCH III modeling system. NOAA/NWS/NCEP/MMAB Tech. Note 281, 15 pp. [Available online at http://polar.ncep.noaa.gov/mmab/papers/tn281/multi_hindanalysis.pdf.]

——, D. Spindler, and H. Tolman, 2011: WAVEWATCH III hindcasts with re-analysis winds. Initial report on model setup. NOAA/NWS/NCEP/MMAB Tech. Note 291, 35 pp. and appendixes. [Available online at http://polar.ncep.noaa.gov/mmab/papers/tn291/MMAB_291.pdf.]

Durrant, T. H., and D. J. M. Greenslade, 2011: Evaluation and implementation of AUSWAVE. CAWCR Tech. Rep. 41, 56 pp. [Available online at http://www.cawcr.gov.au/publications/technicalreports/CTR_041.pdf.]

——, and ——, 2012: Spatial evaluations of ACCESS marine surface winds using scatterometer data. *Aust. Meteor. Oceanogr. J.*, **62**, 263–276.

——, ——, and I. Simmonds, 2013: The effect of statistical wind corrections on global wave forecasts. *Ocean Modell.*, **70**, 116–131, doi:10.1016/j.ocemod.2012.10.006.

——, ——, ——, and F. Woodcock, 2014: Correcting marine surface winds simulated in atmospheric models using spatially and temporally varying linear regression. *Wea. Forecasting*, **29**, 305–330, doi:10.1175/WAF-D-12-00101.1.

Fathauer, T. F., 1975: The Great Bering Sea storms of 9-12 November 1974. *Weatherwise*, **28**, 76–83, doi:10.1080/00431672.1975.9931740.

Francis, O. P., and D. E. Atkinson, 2012a: Synoptic forcing of wave states in the southeast Chukchi Sea, Alaska, at an offshore location. *Nat. Hazards*, **62**, 1169–1189, doi:10.1007/s11069-012-0142-4.

——, and ——, 2012b: Synoptic forcing of wave states in the southeast Chukchi Sea, Alaska, at nearshore locations. *Nat. Hazards*, **62**, 1273–1300, doi:10.1007/s11069-012-0148-y.

Hufford, G., and J. Partain, 2005: Climate change and short-term forecasting for Alaskan northern coasts. *AMS Forum: Living in the Coastal Zone*, San Diego, CA, Amer. Meteor. Soc., 2.3. [Available online at http://ams.confex.com/ams/pdfpapers/83001.pdf.]

Johnson, W. R., and Z. Kowalik, 1986: Modeling of storm surges in the Bering Sea and Norton Sound. *J. Geophys. Res.*, **91**, 5119–5128, doi:10.1029/JC091iC04p05119.

Kowalik, Z., 1984: Storm surges in the Beaufort and Chukchi Seas. *J. Geophys. Res.*, **89**, 10 570–10 578, doi:10.1029/JC089iC06p10570.

Leonard, B. P., 1991: The ULTIMATE conservative difference scheme applied to unsteady one-dimensional advection. *Comput. Methods Appl. Mech. Eng.*, **88**, 17–74, doi:10.1016/0045-7825(91)90232-U.

Lynch, A. H., L. R. Lestak, P. Uotila, E. N. Cassano, and L. Xie, 2008: A factorial analysis of storm surge flooding in Barrow, Alaska. *Mon. Wea. Rev.*, **136**, 898–912, doi:10.1175/2007MWR2121.1.

Mason, O. K., D. K. Salmon, and S. L. Ludwig, 1996: The periodicity of storm surges in the Bering Sea from 1898 to 1993, based on newspaper accounts. *Climatic Change*, **34**, 109–123, doi:10.1007/BF00139256.

Mesquita, M. D. S., D. E. Atkinson, I. Simmonds, K. Keay, and J. Gottschalck, 2009: New perspectives on the synoptic development of the severe October 1992 Nome storm. *Geophys. Res. Lett.*, **36**, L13808, doi:10.1029/2009GL038824.

——, ——, and K. I. Hodges, 2010: Characteristics and variability of storm tracks in the North Pacific, Bering Sea, and Alaska. *J. Climate*, **23**, 294–311, doi:10.1175/2009JCLI3019.1.

Overland, J. E., and C. H. Pease, 1982: Cyclone climatology of the Bering Sea and its relation to sea ice extent. *Mon. Wea. Rev.*, **110**, 5–13, doi:10.1175/1520-0493(1982)110<0005:CCOTBS>2.0.CO;2.

Rodionov, S. N., N. A. Bond, and J. E. Overland, 2007: The Aleutian Low, storm tracks, and winter climate variability in the Bering Sea. *Deep-Sea Res. II*, **54**, 2560–2577, doi:10.1016/j.dsr2.2007.08.002.

Rogers, W. E., and P. A. Wittmann, 2002: Quantifying the role of wind field accuracy in the U.S. Navy's Global Ocean Wave Nowcast/Forecast System. Naval Research Laboratory Tech. Rep. NRL/MR/7320-02-8290, 29 pp. [Available online at http://www.dtic.mil/cgi-bin/GetTRDoc?Location=U2&doc=GetTRDoc.pdf&AD=ADA409540.]

Sallenger, A. H., Jr., 1983: Measurements of debris-line elevations and beach profiles following a major storm: Northern Bering Sea coast of Alaska. U.S. Geologic Survey Open-File Rep. 83-394, 12 pp. [Available online at http://pubs.usgs.gov/of/1983/0394/report.pdf.]

Serreze, M. C., J. E. Box, R. G. Barry, and J. E. Walsh, 1993: Characteristics of Arctic synoptic activity, 1952–1989. *Meteor. Atmos. Phys.*, **51**, 147–164, doi:10.1007/BF01030491.

Simmonds, I., 2015: Comparing and contrasting the behavior of Arctic and Antarctic sea ice over the 35 year period 1979–2013. *Ann. Glaciol.*, **56**, 18–28, doi:10.3189/2015AoG69A909.

——, and I. Rudeva, 2014: A comparison of tracking methods for extreme cyclones in the Arctic basin. *Tellus*, **66A**, 25252, doi:10.3402/tellusa.v66.25252.

——, C. Burke, and K. Keay, 2008: Arctic climate change as manifest in cyclone behavior. *J. Climate*, **21**, 5777–5796, doi:10.1175/2008JCLI2366.1.

Spindler, D. M., and H. Tolman, 2010: Example of WAVEWATCH III for the Alaska area. NOAA/NWS/NCEP/MMAB Tech. Note 266, 17 pp. [Available online at http://polar.ncep.noaa.gov/mmab/papers/tn266/MMAB266.pdf.]

Stopa, J. E., and K. F. Cheung, 2014: Intercomparison of wind and wave data from the ECMWF Reanalysis Interim and the NCEP Climate Forecast System Reanalysis. *Ocean Modell.*, **75**, 65–83, doi:10.1016/j.ocemod.2013.12.006.

NCDC, 1999: Storm Events Database, version 3. NOAA/National Climatic Data Center, accessed 15 March 2015. [Available online at http://www.ncdc.noaa.gov/stormevents/].

Tolman, H. L., 2002: Alleviating the garden sprinkler effect in wind wave models. *Ocean Modell.*, **4**, 269–289, doi:10.1016/S1463-5003(02)00004-5.

——, 2003: Treatment of unresolved islands and ice in wind wave models. *Ocean Modell.*, **5**, 219–231, doi:10.1016/S1463-5003(02)00040-9.

——, 2008: A mosaic approach to wind wave modeling. *Ocean Modell.*, **25**, 35–47, doi:10.1016/j.ocemod.2008.06.005.

——, 2009: User manual and system documentation of WAVEWATCH III version 3.14. NOAA/NWS/NCEP/MMAB Tech. Note 276, 194 pp. and appendixes. [Available online at http://polar.ncep.noaa.gov/mmab/papers/tn276/MMAB_276.pdf.]

——, B. Balasubramaniyan, L. D. Burroughs, D. V. Chalikov, Y. Y. Chao, H. S. Chen, and V. M. Gerald, 2002: Development and implementation of wind-generated ocean surface wave models at NCEP. *Wea. Forecasting*, **17**, 311–333, doi:10.1175/1520-0434(2002)017<0311:DAIOWG>2.0.CO;2.